

Fluorescence Enhancement in Langmuir–Blodgett Films: Role of Amphiphile Structure, Orientation, and Assembly

K. Rajesh, K. Rajendra, and T. P. Radhakrishnan*

School of Chemistry, University of Hyderabad, Hyderabad - 500 046, India

Received: October 4, 2009; Revised Manuscript Received: December 2, 2009

Suppression of self-quenching of fluorescence emission in supramolecular systems is of fundamental interest in the design and development of novel optical materials. While a number of molecular design and assembly strategies have been formulated for the fabrication of molecular crystals with enhanced light emission, parallel explorations based on systematic approaches in the domain of molecular ultrathin films are rare. We have investigated Langmuir–Blodgett films of amphiphilic molecules bearing the same hemicyanine chromophore headgroup but with different possibilities of attachment of the octadecyl hydrocarbon chain, under different deposition conditions. Fluorescence spectroscopy studies indicate enhanced light emission in the derivative with a “tail–head–tail” structure. The observed trends are attributed to the amphiphile structure, nature of deposition, and the chromophore orientations revealed through polarized absorption spectra of the films. The study suggests a simple design strategy toward realization of molecular ultrathin films with enhanced light emission.

Introduction

Aggregation of molecular fluorophores is often accompanied by strong quenching of their fluorescence. As fluorescent molecular materials of interest in applications such as display devices and sensors involve supramolecular assemblies, the adverse impact of these self-quenching effects is a critical problem. Design of molecules and their assemblies aimed at circumventing the quenching effects and realizing enhanced fluorescence in molecular materials is therefore of fundamental relevance. There has been extensive efforts in this direction in the area of molecular crystals.^{1–5} Even though Langmuir–Blodgett (LB) assembly is a simple and elegant methodology that affords fine control on supramolecular assembly and hence is an efficient route to the fabrication of ultrathin films with enhanced material attributes, no systematic approach has been developed to tune fluorescence response through tailoring the amphiphile structure and LB assembly. Fluorescent LB films with several rare-earth metal complexes as well as organic fluorophores have been investigated,^{6–30} and a range of phenomena including quenched or strong fluorescence^{11–13} and electric field and radiation effects on fluorescence^{19,20} in LB films have been reported. Fluorescence of LB films has been attributed to aggregate structures^{14–18} or excimer emission,^{21–23} and extensive time-resolved investigations have been carried out.^{22,24–30} Potential applications of these materials include sensors³¹ as well as probes for film structure²¹ and imaging.³²

Aminostilbazolium (hemicyanine) is a popular fluorophore finding applications as a fluorescence probe³³ and laser dye.³⁴ Incorporated in LB films,^{35–37} it has been an important candidate for molecular electronics³⁸ and quadratic nonlinear optical applications.^{39–52} Optical second harmonic generation (SHG) from LB films based on hemicyanines has been investigated extensively; utility of polyelectrolyte templating in suppressing aggregation effects and stabilizing enhanced response of the films has been demonstrated by us.^{48,49,52} Fluorescence studies

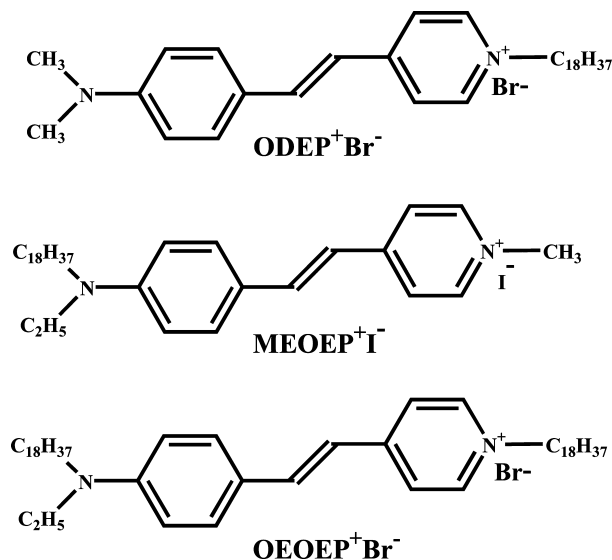


Figure 1. Molecular structure of ODEP⁺Br[−], MEOEP⁺I[−], and OEOEP⁺Br[−].

carried out on LB films of hemicyanines include time-resolved measurements^{36,37} and investigation of the spontaneous formation of H-aggregates.^{14,15,35}

We envisaged that the orientation and organization of the hemicyanine-based amphiphiles at the air–water interface and hence in the LB film will be sensitively dependent on the molecular structure, specifically the mode of attachment of the hydrocarbon chains at the two ends. This would in turn alter the optical responses, while the chromophore unit remained the same. We have focused our investigations on the three amphiphiles shown in Figure 1. *N*-*n*-Alkyl-4-[2-(4-(*N,N*-dimethylamino)phenyl)ethenyl]pyridinium is the hemicyanine system that has been studied extensively earlier,^{34–36,40–52} and the bromide salt of the octadecyl derivative, ODEP⁺Br[−], is shown in Figure 1. *N*-Methyl-4-[2-(4-(*N,N*-ethyloctadecylamino)phenyl)ethenyl]pyridinium iodide (MEOEP⁺I[−]) and *N*-*n*-octadecyl-

* Corresponding author. E-mail: tprsc@uohyd.ernet.in. Phone: 91-40-2313-4827. Fax: 91-40-2301-2460.

4-[2-(4-(*N,N*-ethyloctadecylamino)phenyl)ethenyl]pyridinium bromide (OEOEP⁺Br[−]) find brief mention as members of a series of amphiphiles forming SHG active LB films.⁵³ SHG of some MEOEP⁺I[−] analogues has also been reported.⁵⁴ Dibutylamino as well as alkoxy analogues of OEOEP⁺Br[−] with “tail–head–tail” structure have been shown to form predominantly noncentrosymmetric multilayer LB films capable of strong SHG.⁵⁵ Spectroscopy and epifluorescence microscopy investigations of LB films of the dihexadecylamino analogue of MEOEP⁺I[−] have indicated the formation of aggregate structures.^{14,15} Detailed investigations of Langmuir and LB films of MEOEP⁺I[−] and OEOEP⁺Br[−] and their fluorescence properties have however not been reported. Since OEOEP⁺Br[−] showed interesting structures and behavior at the air–water interface, we present the synthesis and observations on this system in detail. Investigation of the polarization dependence of the electronic absorption spectra provides insight into the chromophore orientations in the different LB films. Comparison of the fluorescence properties of the monolayer LB films of the three amphiphiles possessing identical fluorophore units indicates that LB films of OEOEP⁺Br[−] deposited under specific conditions show 30–50 times enhancement over that of the weakest one based on ODEP⁺Br[−]. We discuss the basis for the enhancement and suggest a possible design strategy toward strongly fluorescent molecular ultrathin films.

Experimental Section

ODEP⁺Br[−] was synthesized following the reported procedure.⁴⁸ We have synthesized OEOEP⁺Br[−] by the condensation of 4-(*N,N*-ethyloctadecylamino)benzaldehyde with 4-methyl-*N*-octadecylpyridinium bromide.⁵⁶ Amounts of 0.37 g (0.87 mmol) of 4-methyl-*N*-octadecylpyridinium bromide and 0.1 mL of piperidine were added to 0.32 g (0.80 mmol) of 4-(*N,N*-ethyloctadecylamino)benzaldehyde in methanol, and the mixture was refluxed for 3 h. OEOEP⁺Br[−] precipitated out as a red crystalline solid on cooling the reaction mixture to 25 °C. The precipitate was filtered, dried, and recrystallized several times from methanol. Yield = 75%; mp/°C = 110; FTIR (KBr): $\bar{\nu}/\text{cm}^{-1}$ = 3044.0, 2916.6, 1572.1, 829.5; ¹H NMR (*d*₆-DMSO) δ/ppm = 8.75 (d, 2H, *J* = 6.8 Hz), 8.04 (d, 2H, *J* = 6.8 Hz), 7.90 (d, 1H, *J* = 16.0 Hz), 7.56 (d, 2H, *J* = 8.8 Hz), 7.12 (d, 1H, *J* = 16.0 Hz), 6.73 (d, 2H, *J* = 8.8 Hz), 4.40 (t, 2H), 3.47 (q, 2H), 3.33 (t, 2H), 1.86 (m, 2H), 1.54 (m, 2H), 1.23 (m, 60H), 1.13 (t, 3H), 0.85 (t, 6H) [where interference due to residual moisture in solvent occurs, the peak positions were determined using the spectrum recorded in CDCl₃]; LC-MS *m/z* = 729 (OEOEP⁺); elemental analysis (calculated for C₅₁H₈₉N₂Br) %C = 75.67 (75.66), %H = 10.98 (11.00), %N = 3.70 (3.46). We have synthesized MEOEP⁺I[−] following a similar procedure as above, employing 4-methyl-*N*-methylpyridinium iodide in place of 4-methyl-*N*-octadecylpyridinium bromide.⁵⁶

Pressure–area isotherms of the amphiphiles at the air–water interface were recorded on a Nima model 611 M LB trough equipped with a Wilhelmy plate for pressure sensing. High purity water (Millipore Milli-Q, resistivity = 18 MΩ·cm, surface tension = 73.0 ± 0.3 mN/m) was used as the subphase. All experiments were carried out at a constant temperature of 25 °C in a clean environment. Solutions of the amphiphiles were prepared in chloroform (Uvasol grade, EMerck) and spread on the aqueous subphase. Our earlier studies on ODEP⁺Br[−] have shown that the extent of aggregation of the headgroups in the Langmuir film is sensitive to the time allowed for equilibration of the monolayer at the air–water interface.^{48,50,51} In the current study, we have ensured that sufficient time (~60 min) was

provided for the monolayer to equilibrate completely at the interface so that molecular aggregation was minimized. The monolayer was then compressed with a barrier speed of 5 cm/min. Hydrophilic quartz/glass substrate for the LB film deposition was prepared by immersing in piranha solution for 6 h followed by sonication and rinsing in high purity water. A freshly cleaved mica plate was also employed as the substrate for depositing LB films. A hydrophobic quartz substrate was prepared by exposing the hydrophilic plate to vapors of hexamethyldisilazane for 12 h. LB films were fabricated by vertical dipping of the substrate at a speed of 5 mm/min. The film transfers of ODEP⁺Br[−] and MEOEP⁺I[−] were carried out on hydrophilic substrates at a surface pressure of 30 mN/m as they collapse above 40 mN/m. The OEOEP⁺Br[−] film was deposited on hydrophilic substrates at two pressures, 30 and 45 mN/m, below and above the plateau in the pressure–area isotherm, respectively. We have attempted the transfer of Langmuir films of the three amphiphiles onto the hydrophobic substrate. The transfer was poor for ODEP⁺Br[−] and MEOEP⁺I[−] as well as OEOEP⁺Br[−] below the plateau, hence they are not considered in this study. However, at 45 mN/m pressure (above the plateau), OEOEP⁺Br[−] could be transferred efficiently. The twin alkyl chain structure and the compact packing at the higher pressure appear to facilitate this. All the experiments described above were repeated on at least 4–5 fresh samples to ascertain the reproducibility of the observations.

Morphology of the Langmuir films at the air–water interface was observed by Brewster angle microscopy (BAM). BAM images of the monolayer were recorded using a Nanofilm model BAM2Plus microscope, and a 532 nm laser beam with a power of 20 mW was used. The films were examined at different stages of compression. Length scales of the images are corrected for the angle of incidence of the beam, and the images presented are 220 × 220 μm² in area. LB films deposited on mica/glass/quartz were imaged using a NT-MDT model Solver Pro M atomic force microscope (AFM) in semicontact mode using a cantilever with force constant of 10 N/m.

Electronic absorption spectra of the LB films deposited on quartz plates (with hydrophilic or hydrophobic surface) were recorded on a Varian model Cary 100 Bio UV–visible spectrometer, and the relevant substrate was used as reference. Polarized absorption spectra were recorded using plane polarized light with the electric vector parallel and perpendicular to the plane of incidence, and sheet polarizers (NSFU-30C, Sigma-Koki) were used for the measurements. A sample was mounted on a goniometer and rotated about the dipping direction, to obtain different angles of incidence of the light, and absorption spectra were corrected for the inclined incidence of light. Orientation of the transition dipole was estimated from the observed linear dichroism following standard procedures.^{56,57} Energies and the associated transition dipole and oscillator strength for electronic transitions in the hemicyanine headgroup and its dimer structures were computed using the semiempirical AM1/CI method, and calculations on the hemicyanine headgroup including solvent effects were carried out using the self-consistent reaction field method.⁵⁶

Steady-state fluorescence excitation and emission spectra of the LB films were recorded on a Horiba Jobin Yvon model Fluorolog-3 spectrofluorimeter in front-face detection geometry. The emission spectra of the films were recorded by exciting them at the λ_{max} of the excitation spectra. Fluorescence polarization measurements were carried out in right-angle geometry, mounting the polarizers in the excitation and emission paths.

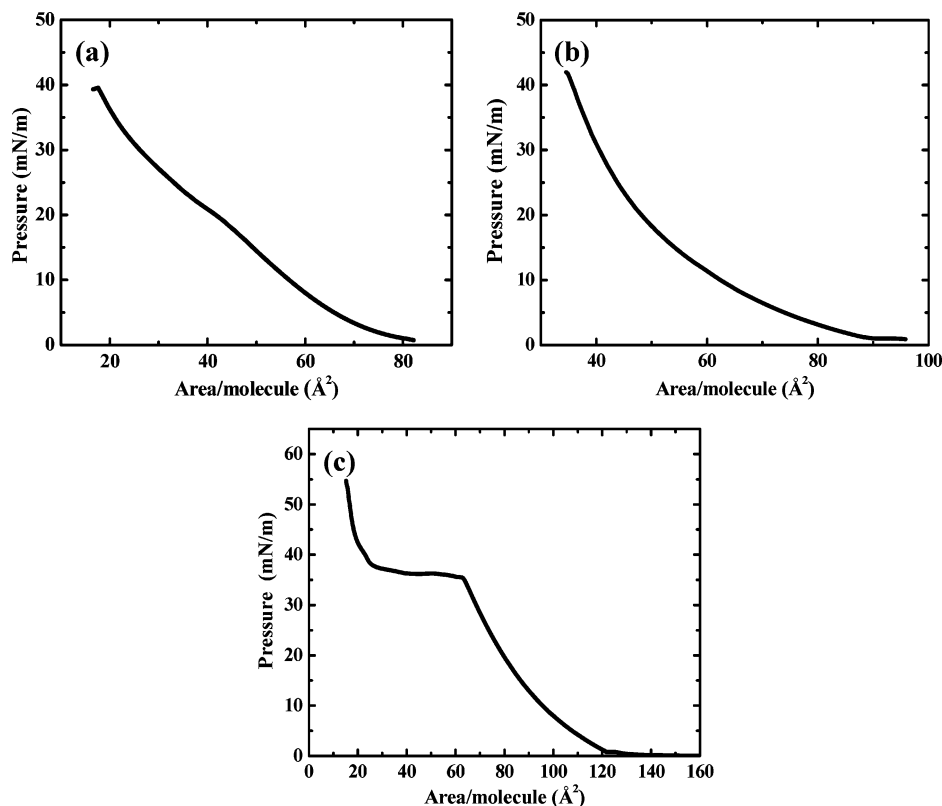


Figure 2. Pressure–area isotherms of the Langmuir films of: (a) ODEP⁺Br[−], (b) MEOEP⁺I[−], and (c) OEOEP⁺Br[−] at the air–water interface at 25 °C.

Results and Discussion

Langmuir films of ODEP⁺Br[−] have been characterized extensively and the impact of polyelectrolytes introduced in the subphase investigated during earlier studies in our laboratory.^{48,49,52} Pressure–area isotherms of ODEP⁺Br[−], MEOEP⁺I[−], and OEOEP⁺Br[−] are shown in Figure 2. The former two are relatively featureless, the liquid expanded phase transforming to a condensed phase smoothly upon compression, and the collapse pressure is ~40–42 mN/m. OEOEP⁺Br[−] on the other hand shows a clear plateau at a pressure of ~36 mN/m and collapse at ~55 mN/m. Extrapolation of the isotherm below and above the plateau indicates molecular areas of 98.6 and 35.1 Å², respectively. This is suggestive of a reorientation of the alkyl chains of the amphiphiles from an oblique to a more vertical disposition occurring at the plateau, and small change in tilt of the headgroup and interdigitation of the chains of neighboring molecules may also occur. BAM imaging of the Langmuir film shows the formation of nearly uniform circular domains as the Langmuir film is compressed across the plateau (Figure 3). Further compression leads to the growth of these domains, their compact packing, and finally coalescence into a nearly homogeneous and continuous film. Analysis of the reflected light intensity suggests an increase in thickness of the film at the air–water interface by ~2 nm during the compression across the plateau.^{56,58,59}

Monolayer LB films were obtained by transfer of the Langmuir films onto substrates with a hydrophilic as well as hydrophobic surface. Only those which showed an appreciable transfer ratio (~0.9 or higher) are considered in the present study (see Experimental Section). The films are designated using the amphiphile name, deposition pressure (in mN/m), and the nature of substrate (hydrophilic = W (water), hydrophobic = O (oil)) as shown in Table 1; the table lists some of the relevant

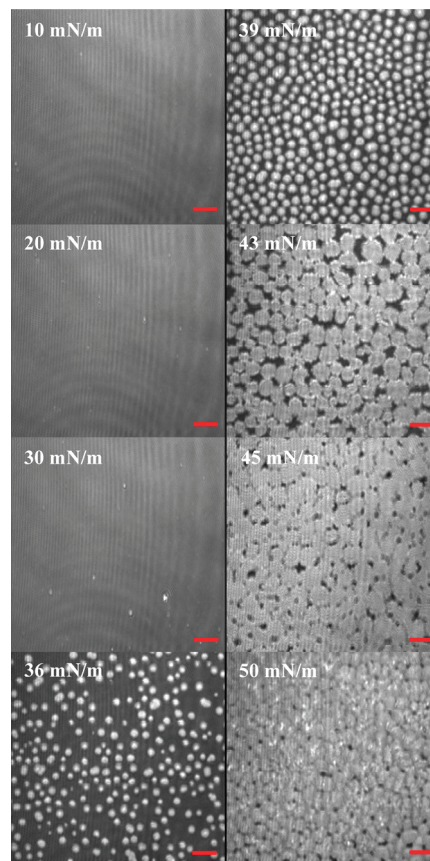


Figure 3. BAM images of the Langmuir film of OEOEP⁺Br[−] at the air–water interface at different surface pressures (scale bar = 25 μm).

characteristics of the films and their deposition. The number of molecules per unit area of the Langmuir films is estimated

TABLE 1: Details of Deposition of the Monolayer LB Films and Molecular Number Density in the Langmuir and LB Films

LB film	amphiphile (Figure 1)	deposition pressure (mN/m)	nature of substrate	transfer ratio	molecules per unit area (nm ⁻²)	
					Langmuir film	LB film
ODEPBr_30_W	ODEP ⁺ Br ⁻	30	hydrophilic	0.90	3.82	3.43
MEOEPI_30_W	MEOEP ⁺ I ⁻	30	hydrophilic	0.93	2.49	2.31
OEOEPBr_30_W	OEOEP ⁺ Br ⁻	30	hydrophilic	0.91	1.45	1.31
OEOEPBr_45_W	OEOEP ⁺ Br ⁻	45	hydrophilic	0.86	5.38	4.62
OEOEPBr_45_O	OEOEP ⁺ Br ⁻	45	hydrophobic	0.87	5.38	4.68

directly from the area/molecule read off the pressure–area isotherms, and at 30 mN/m it decreases in the order ODEP⁺Br⁻, MEOEP⁺I⁻, OEOEP⁺Br⁻. This is consistent with the increase in molecular area from ODEP⁺Br⁻ to MEOEP⁺I⁻ due to the difference in connectivity of alkyl chains and the counterions and the impact of multiple chains and face-on orientation likely in OEOEP⁺Br⁻. The enhanced number density in the Langmuir films at the higher pressure is an obvious consequence of the reorientation of the amphiphiles and more compact packing. The number density in the LB films is estimated from the corresponding values in Langmuir films by scaling with the respective transfer ratios, and the overall trends across the films remain the same.

AFM images of ODEPBr_30_W have been reported earlier,⁴⁹ and they form flower-like structures ~2.0–2.5 nm in thickness, extending over several micrometers. We have reported on multilayer films of ODEP⁺Br⁻ as well in great detail earlier.⁵² In spite of repeated attempts, we found that MEOEPI_30_W as well as OEOEPBr_30_W films are not amenable to satisfactory imaging in the AFM. However, clear images of OEOEPBr_45_W and OEOEPBr_45_O could be recorded. Figure 4 shows the AFM images of the former on mica (hydrophilic surface) and that of the latter on quartz (with hydrophobic surface). OEOEPBr_45_W forms smooth extended films (Figure 4a) with thickness in the range 2.5–3.5 nm, and similar images are obtained for films deposited on glass with a hydrophilic surface.⁵⁶ This is consistent with the likely orientation of the molecule with its headgroup contacting the substrate, perhaps at an angle, and a folded structure with both chains extending outward. OEOEPBr_45_O forms films with a more holey surface (Figure 4b), and the thickness is found to be 5.0–6.0 nm.⁵⁶ This is suggestive of an extended conformation of OEOEP⁺ with one chain contacting the hydrophobic substrate, consistent with the report of Ashwell et al.⁵³ Due to the tail–head–tail structure of OEOEP⁺Br⁻, interaction of the headgroup with the substrate in OEOEPBr_45_W is facilitated by the folded structure, whereas interaction of the tail in OEOEPBr_45_O allows an extended conformation that im-

proves packing and promotes hydrophobic interactions. The differences in the molecular conformations and packing as well as the nature of substrates lead to the observed morphologies of the two films. The conclusions above regarding the orientations of the chains in the two films are supported by the observation of water drops placed on the OEOEPBr_45_W and OEOEPBr_45_O films that indicate the surface of both films to be hydrophobic.

Absorption spectra of the monolayer LB films are collected in Figure 5, and the absorbances at λ_{max} are listed in Table 2. The relatively larger absorbances of the two films deposited above the plateau compared to the other three reflect the higher number density of molecules. All the films show absorption with λ_{max} in the visible range at 460–480 nm. This is the characteristic absorption of the hemicyanine headgroup common to all of them. Solution spectra of the three compounds show λ_{max} in the range 475–510 nm,⁵⁶ and in each case the absorption shifts to the blue with increasing polarity of the solvent; for example, the peaks of ODEP⁺Br⁻ appear at 495 and 476 nm, respectively, in chloroform and acetonitrile. These observations suggest that the local environment of the chromophores in the LB films is fairly polar. AM1/CI computation on the chromophore unit indicates a single strong absorption with λ_{max} at 478.7 nm. When solvation effect due to a polar medium is included in the computation, the absorption maximum is found to shift to the blue; for example, in acetonitrile and dimethylsulfoxide, the λ_{max} is computed to be at ~417 nm.⁵⁶ The trends in the computed absorption characteristics are consistent with the experimental observations and arise due to the large ground state dipole moment of the chromophore. The computation also confirms that the transition dipole coincides with the donor–acceptor dipole axis connecting the N atoms of the dialkylamino and pyridinium groups as expected for an intramolecular charge transfer system.⁵⁶ The spectra of ODEP⁺Br⁻ film and

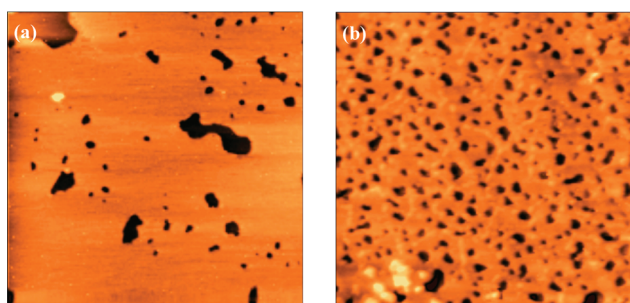


Figure 4. AFM images of the monolayer LB films of: (a) OEOEPBr_45_W on mica (hydrophilic surface) and (b) OEOEPBr_45_O on quartz (with hydrophobic surface). The area of each image is 3 $\mu\text{m} \times 3 \mu\text{m}$.

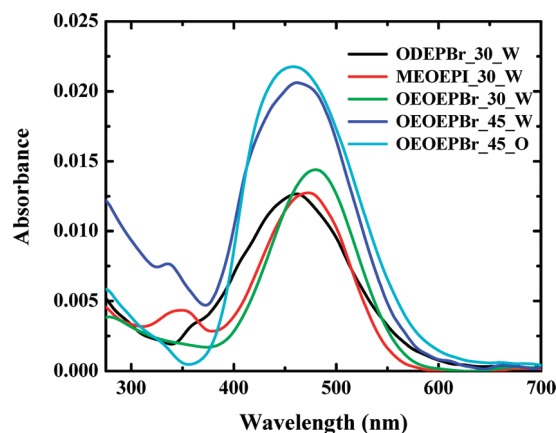


Figure 5. Absorption spectra of monolayer LB films of the hemicyanine-based amphiphiles fabricated under different experimental conditions (see Table 1 for the nomenclature used for the films).

TABLE 2: Absorbance at λ_{\max} of the Monolayer LB Films Measured Using Unpolarized Light (Figure 5) and Orientation of the Transition Dipole of the Headgroup with Respect to the Normal (θ) in the Monolayer LB Films Inferred from the Polarized Absorption Spectra with Light Incident at Different Angles, α (see Figure 6 and Text for Details)

LB film	absorbance at λ_{\max}	α (deg.)	θ (deg.)	
			$\lambda_{\max} \sim$ 410 nm	$\lambda_{\max} \sim$ 470 nm
ODEPBr_30_W	0.012	30	45.0	60.5
		45	49.1	61.6
		60	49.6	61.5
MEOEPI_30_W	0.012	30	-	62.2
		45	-	63.4
		60	-	65.1
OEOEPBr_30_W	0.014	30	-	70.1
		45	-	73.9
		60	-	73.1
OEOEPBr_45_W	0.020	30	53.2	61.9
		45	51.5	60.0
		60	52.8	61.0
OEOEPBr_45_O	0.021	30	52.5	60.2
		45	48.9	60.8
		60	49.9	62.1

OEOEP⁺Br[−] films deposited above the plateau are slightly broader compared to the other two with a weak shoulder emerging at lower wavelengths, and origin of this will be clear from the discussions below.

We have investigated the polarization dependence of the absorption spectra to gain an understanding of the molecular orientations in the various films,⁵⁶ and spectra were recorded by rotating the film about the dipping direction so that light is incident at different angles, α , in both p- and s-polarizations (Figure 6). In all the films, when light is incident normal to the sample plane ($\alpha = 0^\circ$), the absorption shows negligible polarization dependence, whereas linear dichroism is observed when light is incident at an angle ($\alpha \neq 0^\circ$). These observations indicate that the transition dipoles of the chromophores are oriented at some angle (θ) with respect to the normal to the film, but their azimuths (φ) in the film plane have a random distribution. MEOEPI_30_W and OEOEPBr_30_W films showed decreasing intensity for the p-polarized absorption compared to s-polarized absorption, with increasing α angle (spectra of OEOEPBr_30_W are shown in Figure 7).⁵⁶ Interestingly, ODEPBr_30_W, OEOEPBr_45_W, and OEOEPBr_45_O showed broadening and emergence of a blue-shifted second peak in the absorption spectrum, as α was increased from 0° to 60° (spectra of OEOEPBr_45_W are shown in Figure 8). Similar observations on ODEP⁺Br[−] film have been reported earlier.³⁷ Deconvolution of these spectra indicated λ_{\max} at ~ 410 and 470 nm. The peak at 470 nm is due to the hemicyanine headgroup as noted above. The blue-shifted peak is ascribable to H-dimer or aggregate structures in the film,^{37,60} and this is supported by our AM1/CI computations which yielded a λ_{\max} value of ~ 414.7 nm for the parallel dimer of the hemicyanine headgroup.⁵⁶

The angles of orientation of the transition dipole, θ , extracted from the spectra of all the monolayer LB films are collected in Table 2. In the case of ODEPBr_30_W, OEOEPBr_45_W, and OEOEPBr_45_O, the values corresponding to both the wavelengths are listed. The angles estimated suggest that the headgroups of the monomers in ODEPBr_30_W have an average tilt of 61.2° and the aggregates a tilt of 47.9° with respect to the film normal. The orientation and characteristics, slightly different from that reported³⁷ in the earlier study on the dodecyl analogue of ODEP⁺Br[−], may be attributed to the

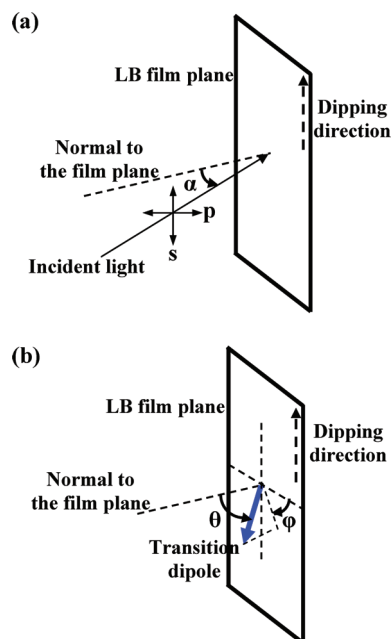


Figure 6. Schematic diagram of the sample geometry used in polarized absorption measurements: (a) orientation of incident light and (b) orientation of the transition dipole (blue arrow) of the chromophore.

changes in the hydrocarbon chain length, temperature, and pH of the subphase and equilibration of the Langmuir film at the air–water interface.^{50,51} The headgroups in the MEOEPI_30_W film show very similar orientation as monomers in the ODEPBr_30_W film with an average tilt of 63.6° . The case of OEOEP⁺Br[−] films is most interesting. The molecular organizations in OEOEPBr_45_W and OEOEPBr_45_O are similar to that in ODEPBr_30_W with the average tilt of monomers being 61.0° and that of the aggregates 52.5° in the former and 61.0° and 50.4° , respectively, in the latter. However, OEOEPBr_30_W is unique in the whole set, with the tilt angle of the headgroups showing the largest value of 72.4° ; there is no sign of aggregation either. This orientation of the headgroups tending toward parallel to the substrate is consistent with the low number density of molecules in the Langmuir as well as LB films of OEOEP⁺Br[−].

The hemicyanine chromophore is known to show strong fluorescence in solution.^{33,34} We have investigated the fluorescence response of the monolayer LB films of the three amphiphiles deposited at 30 mN/m on hydrophilic substrate and that of OEOEP⁺Br[−] deposited at higher pressure and on hydrophobic substrate. The spectra of the five films are collected in Figure 9, and the λ_{\max} of all the films appear in the range 600–630 nm. The spectra shown are those normalized by the absorbance at λ_{\max} for each LB film so that samples with similar optical density are compared. Intensities are shown relative to that of ODEPBr_30_W which shows the weakest fluorescence in the series, and the values at the emission maximum are collected in Table 3. It is well-known that the fluorescence of the ODEP⁺Br[−] film is quenched strongly by aggregation effects.³⁷ The emission intensity of MEOEPI_30_W is found to be approximately 6 times that of ODEPBr_30_W. The significant difference between ODEP⁺Br[−] and MEOEP⁺I[−] is the change of the point of attachment of the hydrocarbon chain with respect to the ionic part of the headgroup. This facilitates better solvation of the headgroup in the Langmuir film of MEOEP⁺I[−] leading to the reduced aggregation reflected in the absorption spectrum of MEOEPI_30_W and the moderate enhancement in the fluorescence emission. The emissions from

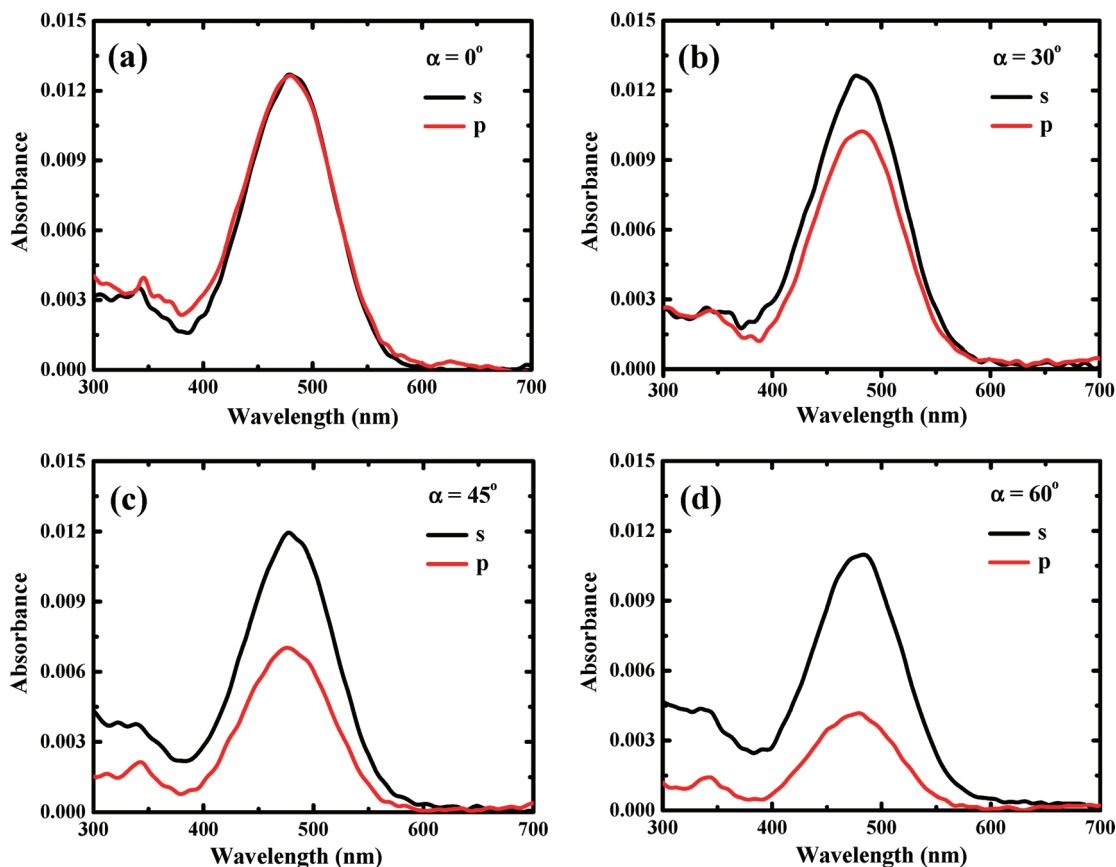


Figure 7. Polarized absorption spectra of the monolayer LB film of OEOEPBr₃₀_W recorded at different angles of incidence, α : (a) 0° , (b) 30° , (c) 45° , and (d) 60° .

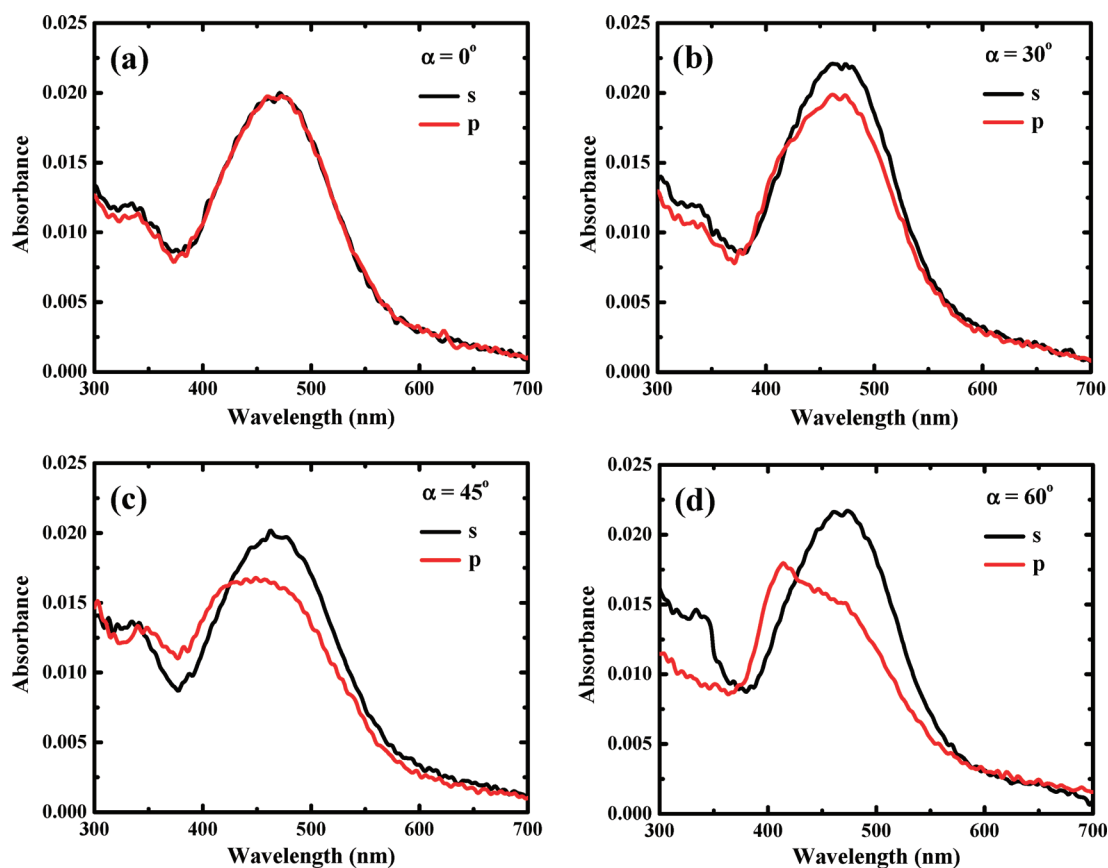


Figure 8. Polarized absorption spectra of the monolayer LB film of OEOEPBr₄₅_W recorded at different angles of incidence, α : (a) 0° , (b) 30° , (c) 45° , and (d) 60° .

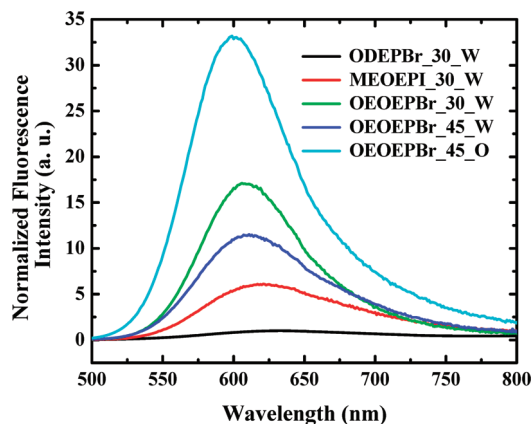


Figure 9. Fluorescence emission spectra of monolayer LB films of the hemicyanine-based amphiphiles (see Table 1 for the nomenclature used for the films). Intensities are normalized by the absorbance at λ_{max} of the respective film, and relative values are shown.

TABLE 3: Intensity at λ_{max} of the Emission Spectrum (In Arbitrary Units) of the Monolayer LB Films, the Intensities Normalized with the Absorbance (Figure 9) as Well as the Number Density of Molecules in the Films, and the Fluorescence Anisotropy Estimated from Fluorescence Polarization Measurements

LB film	fluorescence intensity (arb. units)	relative fluorescence intensity normalized by			fluorescence anisotropy
		absorbance at λ_{max}	number density of molecules		
ODEPBr_30_W	2.6	1.0	1.0		0.13
MEOEPI_30_W	15.8	6.0	8.9		0.12
OEOEPBr_30_W	52.1	17.0	51.9		0.12
OEOEPBr_45_W	45.9	11.0	13.0		0.08
OEOEPBr_45_O	144.9	32.9	40.4		0.09

OEOEPBr_45_W and OEOEPBr_30_W are approximately 11 and 17 times higher than that of ODEPBr_30_W, respectively. In the former, the fluorescence is strong in spite of some aggregation, and this possibly arises due to partial modification of the interaction between the fluorophores by the double hydrocarbon chains. The much stronger emission from the film deposited below the plateau appears to be related to the effective reduction of the interaction of the hemicyanine headgroups by the nearly face-on orientation on the substrate coupled with the separation provided by the hydrocarbon chains attached at both ends. The emission is found to be strongest in OEOEPBr_45_O, about 30 times that of ODEPBr_30_W. In OEOEPBr_45_O, in addition to the conducive molecular packing facilitated by the extended conformation, the attachment of the chains to the hydrophobic substrate and the positioning of the hemicyanine fluorophores away from it possibly suppress any quenching effects due to the substrate. Such phenomena have been discussed earlier in the context of dye molecules adsorbed on glass.⁶¹

Fluorescence intensity normalized with respect to the optical density is meaningful in a photophysical sense as emission related to comparable input of photons is assessed. However, normalization with respect to the number of molecules (i.e., fluorophore units) provides a better comparison from a materials perspective. Table 3 lists also the fluorescence intensity of the different LB films, normalized with respect to the number density of molecules in the LB films. In terms of this number as well, OEOEPBr_30_W and OEOEPBr_45_O show the strongest responses; however, due to the relatively smaller

density of molecules, the efficiency of the former emerges as the highest. This is indirectly related to the more efficient light absorption per molecule exhibited by OEOEPBr_30_W. Measurements of fluorescence polarization⁵⁶ reveal moderate anisotropy⁶² in all the monolayer LB films (Table 3), and this may be attributed to the organized structure of the fluorophores in these ultrathin films.

The present study reveals the significance of structural design of the amphiphiles as well as deposition conditions in determining the fluorescence response of monolayer LB films. In the case of ODEP⁺Br[−] and MEOEP⁺I[−] having a single long hydrocarbon chain, the supramolecular organization and intermolecular interactions are ineffective in suppressing self-quenching effects. In OEOEP⁺Br[−] on the other hand, the long hydrocarbon chains at both ends of the headgroup bestow a tail–head–tail structure that guides the packing of the fluorophore units and controls the intermolecular interactions, leading to minimization of self-quenching effects and enhancement of fluorescence emission. The multiple chains also facilitate efficient assembly of the amphiphiles on a hydrophobic surface which appears to be a simple but effective strategy to elicit maximum fluorescence response from these ultrathin films.

Conclusions

We have characterized the Langmuir film of a novel hemicyanine-based cationic amphiphile with a tail–head–tail structure formed at the air–water interface displaying an organized domain structure. The impact of this amphiphile structure in terms of the attachment of the hydrocarbon chains, on the headgroup orientation and fluorescence properties of the monolayer LB film, is revealed through comparison with other amphiphiles bearing the same headgroup. The significance of the conditions and mode of deposition in realizing strongly fluorescent monolayer LB films is also demonstrated. The current observations suggest a simple molecular design strategy and preferred deposition parameters to realize enhanced optical responses in ultrathin films of fluorescent molecules. Implications of the current findings for other material attributes such as nonlinear optical responses remain to be explored.

Acknowledgment. Financial support from the Department of Science and Technology, New Delhi, and infrastructure support from the Centre for Nanotechnology and Centre for Modelling, Simulation and Design at the University of Hyderabad are acknowledged with gratitude. We thank Mr. B. Balaswamy for help with some of the experiments. KR thanks CSIR, New Delhi, for a senior research fellowship.

Supporting Information Available: Details of synthesis, microscopy, spectroscopy, and computations. This material is available free of charge via the Internet at <http://pubs.acs.org>.

References and Notes

- (1) Wilson, J. N.; Smith, M. D.; Enkelmann, V.; Bunz, U. H. F. *Chem. Commun.* **2004**, 1700.
- (2) Jayanty, S.; Radhakrishnan, T. P. *Chem.—Eur. J.* **2004**, *10*, 791.
- (3) Ren, Y.; Lam, J. W. Y.; Dong, Y.; Tang, B. Z.; Wong, K. S. J. *Phys. Chem. B* **2005**, *109*, 1135.
- (4) Davis, R.; Kumar, N. S. S.; Abraham, S.; Suresh, C. H.; Rath, N. P.; Tamaoki, N.; Das, S. J. *Phys. Chem. C* **2008**, *112*, 2137.
- (5) Hong, Y. N.; Lam, J. W. Y.; Tang, B. Z. *Chem. Commun.* **2009**, 4332.
- (6) Huang, C. H.; Wang, K. Z.; Zhu, X. Y.; Wu, N. Z.; Xu, G. X.; Xu, Y.; Liu, Y. Q.; Zhu, D. B.; Liu, Y. W.; Xue, Z. Q. *Solid State Commun.* **1994**, *90*, 151.
- (7) Huang, H.; Liu, H.; Xue, Q.; Qian, D. *Colloids Surf. A* **1999**, *154*, 327.

- (8) Wang, J.; Wang, H.; Fu, L.; Liu, F.; Zhang, H. *Mater. Sci. Eng. B* **2003**, *B97*, 83.
- (9) Dutta, A. K.; Vanoppen, P.; Jeuris, K.; Grim, P. C. M.; Pevenage, D.; Salesse, C.; De Schryver, F. C. *Langmuir* **1999**, *15*, 607.
- (10) Liu, Y.; Liu, M. *Thin Solid Films* **2002**, *415*, 248.
- (11) Van der Auweraer, M.; Verschuere, B.; De Schryver, F. C. *Langmuir* **1988**, *4*, 583.
- (12) Nagamura, T.; Toyozawa, K.; Kamata, S. *Colloids Surf. A* **1995**, *102*, 31.
- (13) Liu, L.; Liu, Z.; Xu, W.; Xu, H.; Zhang, D.; Zhu, D. *Thin Solid Films* **2006**, *515*, 2596.
- (14) Lusk, A. L.; Bohn, P. W. *Langmuir* **2000**, *16*, 9131.
- (15) Lusk, A. L.; Bohn, P. W. *J. Phys. Chem. B* **2001**, *105*, 462.
- (16) Dutta, A. K. *Langmuir* **1996**, *12*, 5909.
- (17) Parichha, T. K.; Talapatra, G. B. *Opt. Mater.* **1998**, *11*, 9.
- (18) Parichha, T. K.; Talapatra, G. B. *J. Phys. Chem. Solids* **1999**, *60*, 111.
- (19) Itaya, A.; Masuhara, H.; Taniguchi, Y.; Imazeki, S. *Langmuir* **1989**, *5*, 1407.
- (20) Ohta, N.; Ito, T.; Yamazaki, I. *Mol. Cryst. Liq. Cryst. A* **1998**, *314*, 119.
- (21) Murakata, T.; Miyashita, T.; Matsuda, M. *Langmuir* **1986**, *2*, 786.
- (22) Yamazaki, I.; Tamai, N.; Yamazaki, T. *J. Phys. Chem.* **1987**, *91*, 3572.
- (23) Ito, S.; Okubo, H.; Ohmori, S.; Yamamoto, M. *Thin Solid Films* **1989**, *179*, 445.
- (24) Biesmans, G.; Verbeek, G.; Verschuere, B.; Van der Auweraer, M.; De Schryver, F. C. *Thin Solid Films* **1989**, *169*, 127.
- (25) Tamai, N.; Yamazaki, T.; Yamazaki, I. *Thin Solid Films* **1989**, *179*, 451.
- (26) Tamai, N.; Yamazaki, T.; Yamazaki, I. *Can. J. Phys.* **1990**, *68*, 1013.
- (27) Sluch, M. I.; Vitukhnovsky, A. G.; Warren, J. G.; Petty, M. C. *Thin Solid Films* **1992**, *210–211*, 211.
- (28) Ichinose, N.; Nishimura, Y.; Yamazaki, I. *Chem. Phys. Lett.* **1992**, *197*, 364.
- (29) Verma, A. L.; Zhang, Z.; Tamai, N.; Nakashima, K.; Yoneyama, M.; Iriyama, K.; Ozaki, Y. *Langmuir* **1998**, *14*, 4638.
- (30) Zhanga, Z. -J.; Verma, A. L.; Tamai, N.; Nakashima, K.; Yoneyama, M.; Iriyama, K.; Ozakia, Y. *Thin Solid Films* **1998**, *333*, 1.
- (31) Beswick, R. B.; Pitt, C. W. *J. Colloid Interface Sci.* **1988**, *124*, 146.
- (32) Shimomura, M.; Shinohara, E.; Kondo, S.; Tajima, N.; Nagata, Y.; Koshiishi, K. *Sens. Mater.* **1992**, *4*, 29.
- (33) Jones, M. A.; Bohn, P. W. *Anal. Chem.* **2000**, *72*, 3776.
- (34) Zhao, C. F.; Gvishi, R.; Narang, U.; Ruland, G.; Prasad, P. N. *J. Phys. Chem.* **1996**, *100*, 4526.
- (35) Song, Q.; Evans, C. E.; Bohn, P. W. *J. Phys. Chem.* **1993**, *97*, 13736.
- (36) Huang, Y.; Cheng, T.; Li, F.; Luo, C.; Huang, C.; Cai, Z.; Zeng, X.; Zhou, J. *J. Phys. Chem. B* **2002**, *106*, 10031.
- (37) Abraham, E.; Grauby-Heywang, C.; Selector, S.; Jonusauskas, G. *J. Photochem. Photobiol. B* **2008**, *93*, 44.
- (38) Ulman, A. *An Introduction to Ultrathin Organic Films: From Langmuir-Blodgett to Self-Assembly*; Academic Press: Boston, 1991.
- (39) Song, Q.; Xu, Z.; Lu, W.; Bohn, P. W. *Colloids Surf. A* **1994**, *93*, 73.
- (40) Ashwell, G. J.; Hargreaves, R. C.; Baldwin, C. E.; Bahra, G. S.; Brown, C. R. *Nature* **1992**, *357*, 393.
- (41) Girling, I. R.; Cade, N. A.; Kolinsky, P. V.; Jones, R. J.; Peterson, I. R.; Ahmed, M. M.; Neal, D. B.; Petty, M. C.; Roberts, G. G.; Feast, W. J. *J. Opt. Soc. Am. B* **1987**, *4*, 950.
- (42) Scildkraut, J. S.; Penner, T. L.; Willand, C. S.; Ulman, A. *Opt. Lett.* **1988**, *13*, 134.
- (43) Sato, O.; Baba, R.; Hashimoto, K.; Fujishima, A. *J. Phys. Chem.* **1991**, *95*, 9636.
- (44) Carpenter, M. A.; Willand, C. S.; Penner, T. L.; Williams, D. J.; Mukamel, S. *J. Phys. Chem.* **1992**, *96*, 2801.
- (45) Cross, G. H.; Girling, I. R.; Peterson, I. R.; Cade, N. A.; Earls, N. A. *J. Opt. Soc. Am. B* **1987**, *4*, 962.
- (46) Hayden, L. M.; Kowel, S. T.; Srinivasan, M. P. *Opt. Commun.* **1987**, *61*, 351.
- (47) Li, F.; Jin, L.; Huang, C.; Zheng, J.; Guo, J.; Zhao, X.; Liu, T. *Chem. Mater.* **2001**, *13*, 192.
- (48) Chandra, M. S.; Ogata, Y.; Kawamata, J.; Radhakrishnan, T. P. *Langmuir* **2003**, *19*, 10124.
- (49) Chandra, M. S.; Krishna, M. G.; Mimata, H.; Kawamata, J.; Nakamura, T.; Radhakrishnan, T. P. *Adv. Mater.* **2005**, *17*, 1937.
- (50) Chandra, M. S.; Radhakrishnan, T. P. *Mol. Cryst. Liq. Cryst.* **2003**, *403*, 77.
- (51) Chandra, M. S.; Ogata, Y.; Kawamata, J.; Radhakrishnan, T. P. *J. Nonlinear Opt. Phys. Mater.* **2004**, *13*, 347.
- (52) Rajesh, K.; Chandra, M. S.; Hirakawa, S.; Kawamata, J.; Radhakrishnan, T. P. *Langmuir* **2007**, *23*, 8560.
- (53) Ashwell, G. J.; Dyer, A. N.; Lochun, D. *Mol. Cryst. Liq. Cryst.* **1999**, *337*, 421.
- (54) Cross, G. H.; Peterson, I. R.; Girling, I. R.; Cade, N. A.; Goodwin, M. J.; Carr, N.; Sethi, R. S.; Marsden, R.; Gray, G. W.; Lacey, D.; McRoberts, A. M.; Scrowston, R. M.; Toyne, K. J. *Thin Solid Films* **1988**, *156*, 39.
- (55) Ashwell, G. J.; Jackson, P. D.; Crossland, W. A. *Nature* **1994**, *368*, 438.
- (56) See Supporting Information for details.
- (57) N'soukapoé-Kossi, C. N.; Sielewiesiuk, J.; Leblanc, R. M.; Bone, R. A.; Landrum, J. T. *Biochim. Biophys. Acta* **1988**, *940*, 255.
- (58) Patino, J. M. R.; Sanchez, C. C.; Nino, N. M. R. *Langmuir* **1999**, *15*, 2484.
- (59) Winsel, K.; Honing, D.; Lunkenheimer, K.; Geggel, K.; Witt, C. *Eur. Biophys. J.* **2003**, *32*, 544.
- (60) Xu, Z.; Lu, W.; Bohn, P. W. *J. Phys. Chem.* **1995**, *99*, 7154.
- (61) Lee, M.; Kim, J.; Tang, J.; Hochstrasser, R. M. *Chem. Phys. Lett.* **2002**, *359*, 412.
- (62) Togashi, D. M.; Romã, R. I. S.; Gonçalves da Silva, A. M.; Sobral, A. J. F. N.; Costa, S. M. B. *Phys. Chem. Chem. Phys.* **2005**, *7*, 3874.